


## Article

# Optimized Design of Robotic Arm for Tomato Branch Pruning in Greenhouses

Yuhang Ma <sup>1</sup>, Qingchun Feng <sup>2,3,\*</sup> , Yuhuan Sun <sup>2</sup>, Xin Guo <sup>2,3</sup>, Wanhao Zhang <sup>2</sup>, Bowen Wang <sup>2</sup> and Liping Chen <sup>1,2,3,\*</sup>

<sup>1</sup> School of Mechanical Engineering, Guangxi University, Nanning 530004, China; 2111391077@st.gxu.edu.cn

<sup>2</sup> Intelligent Equipment Research Center, Beijing Academy of Agriculture and Forestry Sciences, Beijing 100097, China

<sup>3</sup> National Research Center of Intelligent Equipment for Agriculture, Beijing 100097, China

\* Correspondence: fengqc@nercita.org.cn (Q.F.); chenlp@nercita.org.cn (L.C.)

**Abstract:** Aiming at the robotic pruning of tomatoes in greenhouses, a new PRRPR configuration robotic arm consisting of two prismatic (P) joints and three revolute (R) joints was designed to locate the end effector to handle randomly growing branches with an appropriate posture. In view of the various spatial posture of the branches, drawing on the skill of manual pruning operation, we propose a description method of the optimal operation posture of the pruning end effector, proposing a method of solving the inverse kinematics of the pruning arm based on the multi-objective optimization algorithm. According to the spatial distribution characteristics of the tomato branches along the main stem, the robotic arm structure is compact and the reachable space is maximized as the objective function, and a method of optimizing the key geometric parameters of the robotic arm is proposed. The optimal maximum length of the arm's horizontal slide joint was determined to be 953.149 mm and the extension maximum length of its telescopic joint was 632.320 mm. The verification test of the optimal structural parameter showed that the optimized robotic arm could reach more than 89.94% of the branches in the pruning target area with a posture that meets the pruning requirements. This study is supposed to provide technical support for the development of a tomato pruning robot.

**Keywords:** agricultural robot; tomato pruning; manipulator; structural optimization



**Citation:** Ma, Y.; Feng, Q.; Sun, Y.; Guo, X.; Zhang, W.; Wang, B.; Chen, L. Optimized Design of Robotic Arm for Tomato Branch Pruning in Greenhouses. *Agriculture* **2024**, *14*, 359. <https://doi.org/10.3390/agriculture14030359>

Academic Editor: Antonio Valente

Received: 15 January 2024

Revised: 13 February 2024

Accepted: 22 February 2024

Published: 23 February 2024



**Copyright:** © 2024 by the authors. Licensee MDPI, Basel, Switzerland. This article is an open access article distributed under the terms and conditions of the Creative Commons Attribution (CC BY) license (<https://creativecommons.org/licenses/by/4.0/>).

## 1. Introduction

The tomato is extensively cultivated globally with enormous demands for consumption and a large cultivation scale [1,2]. The tomato is a herbaceous plant with sympodial branching, where each leaf axil can produce lateral buds to form branches, on which secondary branches can grow, and so forth [3–5]. Without proper pruning, plants can become overly bushy, affecting ventilation and light penetration, even leading to pests and diseases. It also consumes ample nutrients, inhibiting fruit growth and quality. So, redundant branches need timely removal [6–8].

In industrial greenhouse, plant pruning is performed for almost the entire tomato production cycle, which lasts around 8–9 months. This work is complex with a low efficiency and mechanization rate, consuming 40–60% of the total labor costs. Therefore, developing a tomato defoliation pruning robot to replace manual pruning is of great significance to improve the economic benefits of greenhouse tomatoes [9,10].

Pruning robots for crops like grapevines [11], fruit trees [12–14], poplar [15], cherry tomato [16], rose bushes [17], bell pepper [18], etc. are current hot topics in agricultural robotics. The key component, the robotic pruning arm, is responsible for positioning the end effector at the target. Considering the random and irregular pose of branch growth, the spatial reachability of the pruning arm significantly impacts the robot's performance. Current pruning robots mainly employ standard industrial arms. However, the limited

space between dense tomato bushes for robot operation and the need for low-cost arms in agricultural robots pose difficulties for industrial arms to meet both operational space and structural compactness requirements in greenhouses with randomly distributed plants. Therefore, a dedicated tomato pruning arm must be designed with optimized structure parameters to enable the precise and efficient operation of tomato pruning robots [19].

There have been extensive studies by numerous researchers at home and abroad on designing and optimizing robotic arm configurations for agricultural applications. To facilitate camellia pollen harvesting using a group of 4-DOF RRRR robotic arms, Zhao, qing et al. simplified the target space and optimized the upper arm length, forearm length and forearm rotation angle by minimizing the harvesting space interval. Using the interior point method in an optimization toolbox, they obtained optimal arm lengths of 592 mm and 638 mm, and a minimum forearm rotation angle of  $16^\circ$  [20]. To effectively cover the large workspace of tall fruit trees using a compact dual-arm mechanism, Xiong et al. set the optimization objectives as minimal workspace redundancy and compact arm structure. They adopted the NSGA-II algorithm to optimize the extension lengths and maximum pitch angles of two PPP-configured apple harvesting robotic arms, obtaining optimized lengths of 1119.3 mm and 898.7 mm for the two arms, and horizontal pitch angles of  $39.4^\circ$  and  $26^\circ$ , respectively [21]. Targeting cucumber harvesting needs in fields, Feng et al. analyzed the workspace of a 5-DOF cucumber harvesting robot, and optimized the upper arm, lower arm and end effector lengths by maximizing the effective workspace and minimizing structural lengths. Using graphical geometry optimization, they obtained optimized lengths of 236 mm, 443 mm and 370 mm, respectively [22]. Faezeh Molaei modeled orchard environments, focusing on the manipulability and isotropy of arms, and optimized the second and third link lengths of a 7-DOF industrial robotic arm for grapevine pruning using NSGA-II, resulting in equal lengths of 0.7 m for both links [23]. Ali Roshanianfard et al. optimized a robotic arm for harvesting heavyweight crops. Considering the depth of the field and cost, they designed a 4-DOF PRRR arm and chose the second, third and fourth link lengths as 500 mm, 1200 mm and 1200 mm, respectively, for workspace coverage [24].

However, current agricultural robotic arms abstract the target object simply as a specified point in space during their design, with the sole goal of reaching the spatial point. For tomato branches, on top of avoiding fruit and main stem damage, the cut surface must closely conform to the main stem to prevent pests and diseases. The target growth direction must also be considered comprehensively based on the working point.

Targeting the intelligent pruning needs in factory tomato cultivation, this paper designs a dedicated tomato pruning robotic arm. Considering the reliable operation requirements for branches with different poses, factors like the branch operation posture, reachability and compactness are synthetically taken into account to determine the optimal geometric parameters using multi-objective optimization algorithms, providing insights for the development of tomato pruning robots. The main contributions are as follows:

- (1) A dedicated PRRPR configuration robotic arm for tomato plant pruning was designed, according to the branch growth form and the manual pruning operation requirement.
- (2) In view of the requirement of pruning at the branch's bottom with less stubble to avoid incision infection, the optimal pruning posture of the robotic arm end was defined, which has not been addressed in the current research related to this topic. With the optimal pruning posture as the objective, the kinematic model of the robotic arm was established based on the objective optimization algorithm, so as to obtain a better pruning efficiency.
- (3) With the most compact structure and the highest reachability as the objective, the key link length parameters of the robotic arm were determined, and the optimal configuration was verified through simulating the end effector's reachability for the branches with various postures.

This paper is organized as follows. The tomato pruning operation principle is presented in the next section. A robotic arm is designed according to this principle, and its configuration and kinematic model are described in Section 3. In Section 4, the structural parameters of the robotic arm are optimized and the effectiveness of the optimization results is verified by experiments in Section 5. Finally, some conclusions are given, and the limitations of the current scheme and the next steps of work and improvement are introduced. The overview of the research in this paper is shown in Figure 1.

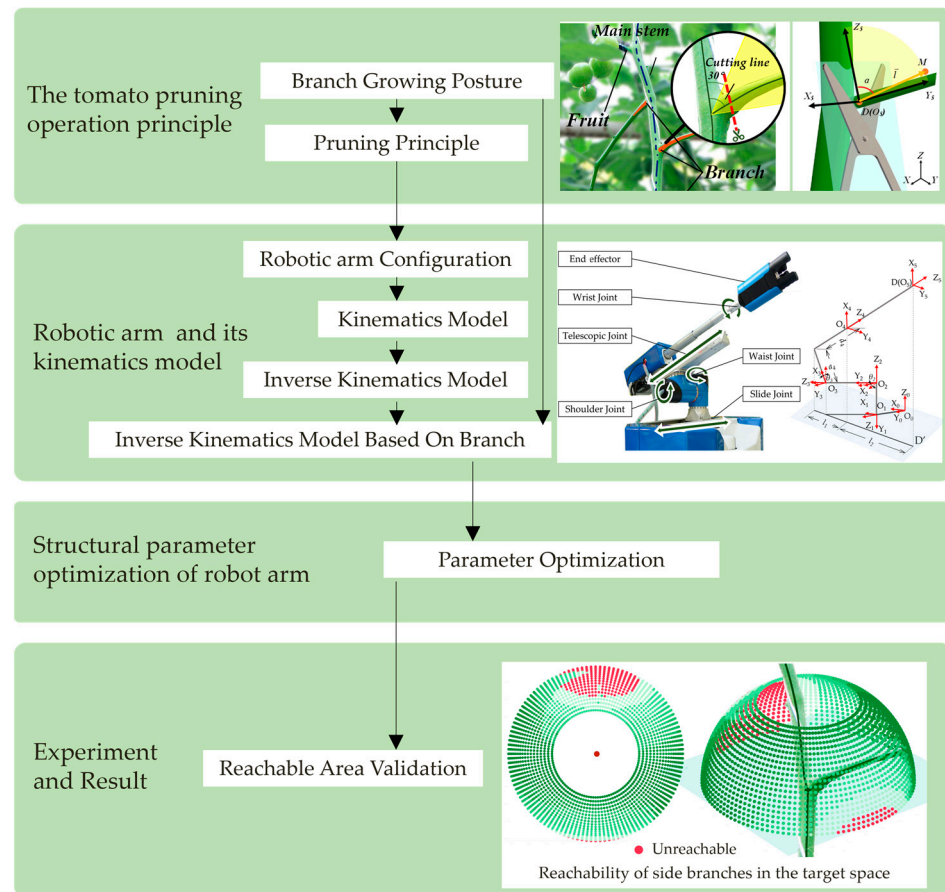
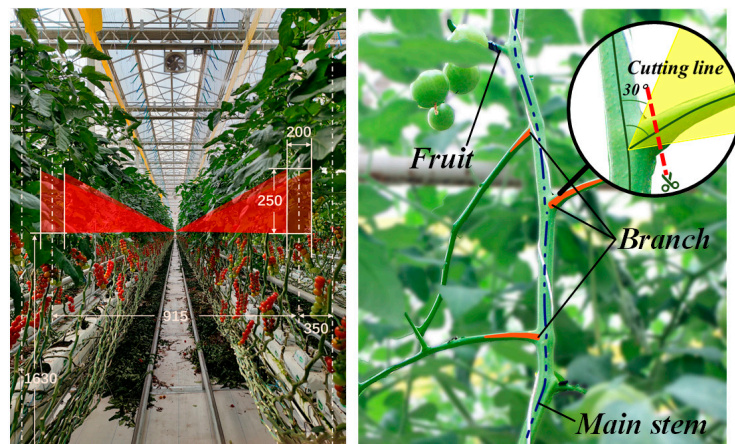


**Figure 1.** Overview of optimized design of pruning arm.

## 2. Tomato Pruning Operation Principle

### 2.1. Industrial Greenhouse Environment

Greenhouse tomato cultivation environments are characterized by factory-based, intensive and standardized features. As shown in Figure 2a, the greenhouse tomato cultivation environment has a row spacing of 915 mm and plant spacing of 250 mm, facilitating robot maneuvering on the rail between rows. When tomato plants grow to 40–50 cm in height, trimming is required. Afterwards, tomato growth maintains a certain regularity and stability, with the pruning area stably keeping within 1630–1880 mm above the ground, providing necessary environmental conditions for researching tomato automation.



(a) Tomato pruning area in industrial greenhouse (b) Branch growth form

Figure 2. Work conditions and branch target of robotic pruning.

2.2. Pruning Operation Requirements

Branches grow staggered along the main stem with varied poses and shapes, as shown in Figure 2b. Occurring below main stem nodes, branches grow in a disorderly manner around the stem. Through manual measurement in the greenhouse, and also taking into account the pruning requirements of the greenhouse, we obtained that the branches that need pruning open 30°–90° relative to the main stem, with diameters of 5–10 mm. To avoid long stubble infecting plants, Pruning Process Standards require pruning tightly against the plant’s main stem with stubble less than 5 mm, and smooth residue-free cross-sections. To meet these horticultural requirements while ensuring cutting success, the branch direction needs to be determined when considering the pruning point.

2.3. Branches Spatial Pose

Robotic pruning requires not only position but also spatial pose information of the branches. Thus, a spatial vector is used to represent the branch pose, as shown in Figure 3. The vector origin  $D(x_t, y_t, z_t)$  is 5 mm away from the main stem along the branch, which is also the pruning point. The end point  $M(x_m, y_m, z_m)$  is 3 cm outward along the growth direction from  $D$ . Connecting  $D$  and  $M$  gives vector  $\vec{DM}$ , which, after normalization, produces the unit direction vector of the branch:

$$\vec{l}(m_x, m_y, m_z)$$

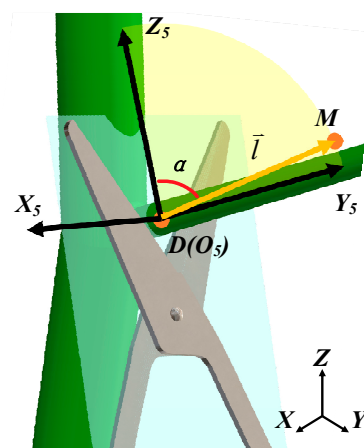


Figure 3. Pose relation of branch and pruning end effector.

Based on the point  $D$  and the direction vector  $\vec{l}$  of the branch, the pose of the branch in the camera field of view can be defined to further solve the pose matrix of the robotic arm end effector.

#### 2.4. Description of Optimal Grasping Posture

The desired end effector pose matrix can be obtained based on the defined branch pose. To ensure pruning reachability, the angle between the pruning shear plane and branch direction should be maximized, i.e., the larger the angle between the plane vectors, the easier it is to obtain a smooth shear plane without residues, and the higher the reachability. Meanwhile, the branch receives minimum positive tension on the normal plane of the shears, making it easier to cut. Considering the requirement that the shear tip must coincide with the pruning point, the optimal end effector pose for a branch pose in pruning is defined as follows: the opening direction  $Z_5$  of the pruning shear has the maximum angle  $\alpha$  with the branch direction vector  $\vec{l}$ ; the  $X_5$  axis on the pruning shear plane is perpendicular to  $\vec{l}$ , i.e.,  $90^\circ$ ; the pruning point  $D$  coincides with the pruning shear point  $O_5$ .

Based on the end effector pose: when the angle between the tomato branch and shear plane is greater than  $30^\circ$ , the end effector can effectively complete branch pruning. When the angle is less than  $30^\circ$ , the reachability and effect of pruning decrease significantly. Thus, an absolute value greater than  $30^\circ$  for the end branch angle  $\alpha$  is set as a necessary condition for pruning.

The desired end effector pose is defined by the expressions of the three axial unit vectors of the coordinate system  $\{U\}$  attached to the arm end against the base coordinate system, as shown in Figure 3. In the end effector coordinate system  $O_5-X_5Y_5Z_5$ ,  $O_5$  coincides with  $D$ . Let the  $Z_5$  axis direction vector be  $\vec{Z}_5$ ; the  $X_5$  axis is perpendicular to  $Z_5$  axis and the plane containing the branch direction vector  $\vec{l}$ , denoted as  $\vec{X}_5 = \vec{l} \times \vec{Z}_5$ ; then, the  $Y_5$  axis direction vector  $\vec{Y}_5 = \vec{Z}_5 \times \vec{X}_5$  can be determined. Once the  $Z$ -axis direction vector is fixed, the three main axial vectors  $O_5-X_5Y_5Z_5$  can be determined. When the end effector reaches the target point with  $O_5$  coinciding with the pruning point, only the  $M$  point coordinates on the tomato branch are needed to obtain the  $Z$ -axis direction vector, thereby deriving the optimal end effector pose for this branch state.

### 3. Kinematic Model of Pruning Arm

#### 3.1. Structural Design of Pruning Arm

The pruning arm needs to meet two requirements: first, it must be able to accurately locate the spatial point of the branch; second, it must be able to prune with a proper operating posture, with the angle between the end effector and the branch vector greater than 30 degrees. Therefore, the pruning arm requires at least 4 degrees of freedom. Considering cost-effectiveness, this paper adopts a 4-DOF manipulator. Since the branches are distributed over a large height range, the arm needs a relatively large workspace. If all four joints use rotational joints, the pose of the arm will change as the joints rotate, which can easily interfere with the dense surrounding plants and affect the pruning efficiency and safety. On the other hand, the space required to accommodate prismatic joints is limited. Therefore, this paper selects a robotic arm structure combining prismatic and rotational joints, so that the manipulator can ensure reachability while improving flexibility and stability. Additionally, because the tomato branches grow upwards overall, pruning deeply from the bottom can obtain better operating space. Therefore, an upward-looking PRRPR robotic arm was constructed to perform the tomato pruning work. (Figure 4a).

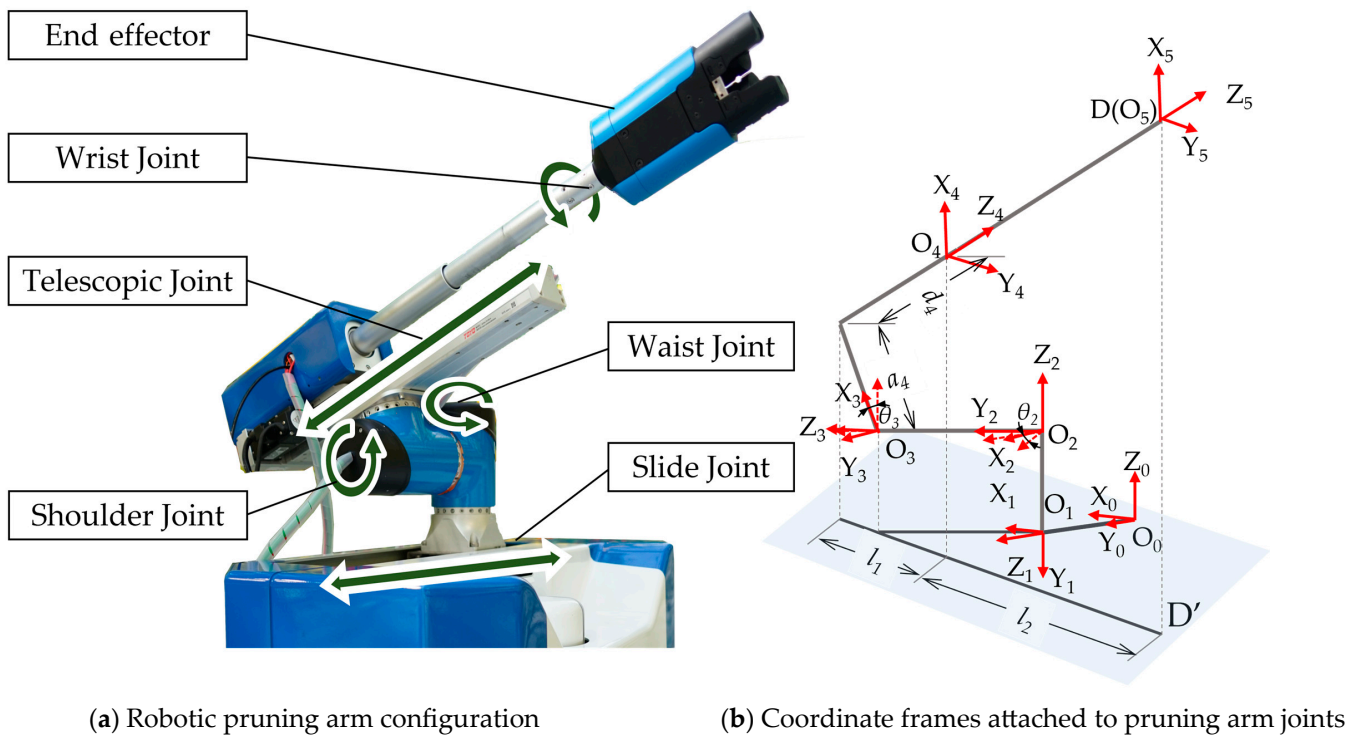


**Figure 4.** Robotic pruning robotic arm configuration and its coordinate frames.

As shown in Figure 5, the direction of the sliding joint is the same as the direction of the tomato plants' line. The waist joint rotates the arm left/right while the shoulder joint elevates it up/down. The telescopic joint extends/retracts the end effector along the depth direction. The wrist joint rotates the end effector shear plane to better fit the tomato branch. Finally, the pruning end effector reaches the desired pruning position, and the end effector performs the pruning of the branches.

According to the robotic principles for establishing coordinate frames, the frames attached to the joints are set up as shown in Figure 4b. The DH parameters of the robotic arm are given in Table 1:

**Table 1.** DH parameters of the pruning robotic arm.

$i$	$\alpha_{i-1}$	$a_{i-1}$	$d_i$	$\theta_i$
1	$-\pi/2$	0	$d_1$	0
2	$\pi/2$	0	137.5	$\theta_2$
3	$-\pi/2$	0	122	$\theta_3$
4	$\pi/2$	172.5	$d_4$	0
5	0	0	390	$\theta_5$

Here,  $d_1$  is the movement of the sliding joint,  $\theta_2$  and  $\theta_3$  are the rotational angles of the waist and shoulder joints, respectively,  $d_4$  is the movement of the telescopic joint,  $\theta_5$  is the rotational angle of the wrist joint, and the numerical range of motion of each robotic arm joint is

$$\begin{cases} 0 \leq d_1 \leq 320(\text{mm}) \\ -\pi/2 \leq \theta_2 \leq \pi/2 \\ 0 \leq \theta_3 < \pi/2 \\ 0 \leq d_4 \leq 440 \\ 0 \leq \theta_5 \leq \pi \end{cases}$$

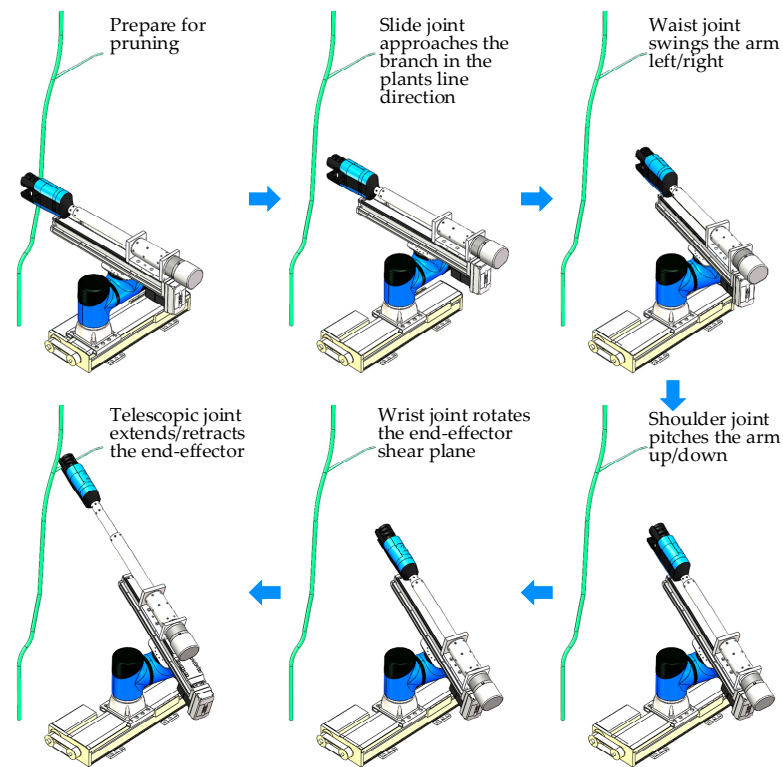


Figure 5. Robotic pruning process.

### 3.2. Forward Kinematic Model

The Z-axis direction vector of the end pose is derived from the joint variables and pruning point. The coordinate origin  $O_3(d_1 + d_3\cos(\theta_2), d_3\cos(\theta_2), d_2)$  of the shoulder joint frame is represented in the base frame, which is used to solve the coordinates  $O_4(x_4, y_4, z_4)$  of the telescopic joint frame origin in the base frame. When projecting onto the base frame XOY plane, the projected coordinates of the pruning point are  $D'(x_t, y_t, 0)$ ; the projected coordinates of the telescopic joint origin are  $O_4'(x_e, y_e, 0)$ ; the projected coordinates of the shoulder origin are  $O_3'(d_1 + d_3\cos(\theta_2), d_3\cos(\theta_2), 0)$ ; the slope of the projection line  $l_1$  of the telescopic joint is

$$k = \begin{cases} \tan(\theta_2 + \pi/2) & (\theta_2 < 0) \\ \tan(\pi - \theta_2) & (\theta_2 > 0) \end{cases} \quad (1)$$

Using the point-slope form, the projection line  $l_1$  of the telescopic joint is determined as  $y = kx + b$ . Line  $l_1$  passes through point  $O_4'$ , so the intercept of line  $l_1$  can be obtained as

$$b = d_3 \sin(\theta_2) - k(d_1 + d_3 \cos(\theta_2)) \quad (2)$$

When the shoulder pitch angle is  $\theta_3$ , the link offset  $a_4$  projects onto line  $l_1$  as  $l_2 = a_4\sin(\theta_3)$ , which is then used to obtain the coordinates of  $O_4'$ , and finally, the coordinates of the telescopic joint origin  $O_4$  in the base frame:

$$\begin{cases} x_4 = (d_1 + d_3 \cos(\theta_2)) \mp l_2 / \sqrt{1 + k^2} \\ y_4 = kx_e + b \\ z_4 = d_2 + a_4 \cos(\theta_3) \end{cases} \quad (3)$$

Vector  $\vec{O_4D}$  is the Z-axis direction vector  ${}^R_5\vec{Z} = (x_t - x_4, y_t - y_4, z_t - z_4)$  of the end effector working pose. Normalizing gives the unit Z-axis direction vector  $L = (n_x, n_y, n_z)$ . Substituting into Equations (1)–(3) gives

$$\begin{cases} n_x = A \mp B \\ n_y = (y_t - d_3 \sin(\theta_1))(A \mp B) / A \\ n_z = z_t - d_2 - a_4 \cos(\theta_2) \end{cases} \quad (4)$$

where  $A = x_t - d_1 - d_3 \cos(\theta_2)$ ,  $B = (a_4 \sin(\theta_3)) / \sqrt{((y_t - d_3 \sin(\theta_2))^2 / A^2) + 1}$ .

If the X-axis of the end pose is perpendicular to the Z-axis and the vector  $\vec{n}$  of the branch lies on a plane perpendicular to the Z-axis, then the direction vector of the X-axis is

$${}^R_5\vec{X} = \vec{l} \times \vec{L} \quad (5)$$

The direction vector of the Y-axis can be determined by the X-axis and the Z-axis:

$${}^R_5\vec{Y} = \vec{L} \times {}^R_5\vec{X} \quad (6)$$

According to Equations (4)–(6), the vector expressions of  $\vec{X}$ ,  $\vec{Y}$  and  $\vec{Z}$  of the end pose coordinate axis in the robot base coordinate system can be finally determined, and the end pose matrix  ${}^0_5R$  can be obtained by arranging the three main axis direction vectors:

$${}^0_5R = \begin{bmatrix} \vec{X} & \vec{Y} & \vec{Z} \end{bmatrix} = \begin{bmatrix} \vec{X}_x & \vec{Y}_x & \vec{Z}_x \\ \vec{X}_y & \vec{Y}_y & \vec{Z}_y \\ \vec{X}_z & \vec{Y}_z & \vec{Z}_z \end{bmatrix}$$

Adding the position component  $t_f = [x_t, y_t, z_t]^T$  of the end effector to obtain the pose matrix  $T_F$  of the end effector of the robot operation based on the pose derivation of the tomato branch:

$$T_F = \begin{bmatrix} {}^0_5R & t_f \\ 0 & 1 \end{bmatrix} = \begin{bmatrix} m_y n_z - m_z n_y & n_y(m_x n_y - m_y n_x) - n_z(m_z n_x - m_x n_z) & n_x & x_t \\ m_z n_x - m_x n_z & n_x(m_x n_y - m_y n_x) - n_z(m_y n_z - m_z n_y) & n_y & y_t \\ m_x n_y - m_y n_x & n_y(m_y n_z - m_z n_y) - n_x(m_z n_x - m_x n_z) & n_z & z_t \\ 0 & 0 & 0 & 1 \end{bmatrix}$$

### 3.3. Inverse Kinematic Model

The establishment of the kinematic model is the basis for controlling the robotic arm. According to the principle of coordinate transformation and DH parameters, there is the following transformation relationship between adjacent coordinate systems:

$${}^{i-1}_i T = \begin{bmatrix} c\theta_i & -s\theta_i & 0 & a_{i-1} \\ s\theta_i c\alpha_{i-1} & c\theta_i c\alpha_{i-1} & -s\alpha_{i-1} & -s\alpha_{i-1} d_i \\ s\theta_i s\alpha_{i-1} & c\theta_i s\alpha_{i-1} & c\alpha_{i-1} & c\alpha_{i-1} d_i \\ 0 & 0 & 0 & 1 \end{bmatrix} \quad (7)$$

By substituting the DH parameters into Equation (7), the transformation matrix between adjacent joints can be obtained. In the equation,  $s = \sin$ ,  $c = \cos$ . By continuously multiplying the transformation matrices of the adjacent coordinate systems from right to left, the transformation matrix of the robot end relative to the robot base can be obtained:

$${}^0_5 T = {}^0_1 T \cdot {}^1_2 T \cdot {}^2_3 T \cdot {}^3_4 T \cdot {}^4_5 T \quad (8)$$

Equation (8) is the forward kinematics of the whole branch operation robotic arm. To control the robotic arm, the inverse kinematics of the robotic arm also need to be analyzed [25]. The inverse kinematics solution process of the robotic arm is as follows. After multiplying the inverse matrix of the transformation from joint 1 to joint 0 by the



forward kinematics transformation matrix from the left, the equation relationship shown in Equation (9) is established:

$$({}^0_1T)^{-1} {}^0_5T = {}^1_2T {}^2_3T {}^3_4T {}^4_5T \tag{9}$$

By simplifying and solving Equation (9), the inverse solutions of each joint of the robotic arm can be obtained. Subject to the configuration and joint limit settings of the robotic arm, there is only one set of inverse solutions for a given end pose. The inverse solution results are

$$\begin{cases} d_1 = d_3c_2 + d_1 + a_4c_3s_2 + (d_4 + d_5)s_2s_3 - [d_3c_2 + a_4c_3s_2 + (d_4 + d_5)s_2s_3] \\ \theta_2 = a \tan 2(s_2s_3, c_2s_3) \\ \theta_3 = a \tan 2(c_2s_3, c_3c_2) \\ d_4 = (d_2 + (d_4 + d_5)c_3 - a_4s_3 + a_4s_3 - d_2) / c_3 - d_5 \\ \theta_5 = -a \tan 2(s_3s_5 / -c_5s_3) \end{cases} \tag{10}$$

Equation (10) describes the inverse kinematics solutions of the whole branch robotic arm. At this time, only the desired pose matrix of the end effector needs to be determined to obtain the amount of motion of each joint. In Section 2.4, according to the optimal grasping pose defined by the tomato branch pose, it is a series of poses. By optimizing the solution, the unique optimal end pose matrix for different branch situations can be obtained.

### 3.4. Inverse Kinematic Model for the Optimal Pruning Posture

The desired end pose of the robotic arm is not unique for different tomato branch growth forms, and the ideal solution cannot be obtained for special growth situations. At this time, the theoretical end pose angle  $\alpha$  maximum situation is selected as the optimal solution. The expression form of the Z-axis of the end coordinate system is abbreviated as follows by Equation (11):

$$\vec{L}_Z(n_x, n_y, n_z) \tag{11}$$

The angle  $\alpha$  between the normal vector of the end effector and the direction vector of the tomato branch can be expressed as

$$\alpha = \cos^{-1} \left( \frac{\vec{l} \cdot \vec{m}}{|\vec{l}| |\vec{m}|} \right) \tag{12}$$

According to Equation (12), the size of the angle  $\alpha$  is only related to the pose of the tomato branch and  $d_1$ ,  $\theta_2$  and  $\theta_3$ , so the optimization objective for the angle  $\alpha$  can be written as

$$\min f_\alpha = -\alpha(d_1, \theta_2, \theta_3) \tag{13}$$

As long as  $d_1$ ,  $\theta_2$  and  $\theta_3$  are obtained by optimizing and solving Equation (13), the end pose matrix can be uniquely determined by substituting them into Equation (8), and the matrix is substituted into Equation (10) to realize the control of the whole branch robotic arm. According to the actual situation, the constraint conditions of the variables  $d_1$ ,  $\theta_2$  and  $\theta_3$  are

$$s.t. \begin{cases} 0 \leq d_1 \leq d_{1max} \\ -\pi/2 \leq \theta_2 \leq \pi/2 \\ 0 \leq \theta_3 < \pi/2 \\ \theta_2 = f_{\theta_2}(d_1) \\ \theta_3 = f_{\theta_3}(d_1, \theta_1) \end{cases}$$

To solve this nonlinear constrained optimization problem, first transform it into an unconstrained problem by using the penalty function method, and introduce penalty terms to restrict the solutions that do not satisfy the constraint conditions [26]; use the boundary phase method to approximate a minimum value interval, input the initial values of each

variable to obtain an interval containing the global minimum value as the initial value of the subsequent steps, avoid falling into the local minimum situation, and improve the solution accuracy and efficiency.

Apply the golden section method to gradually reduce the minimum value and the minimum value interval in the interval obtained in the previous step, greatly reduce the calculation amount of the subsequent steps, ensure the convergence speed and accuracy, and avoid the difficulty of obtaining partial derivatives for complex equations [27]. After obtaining a smaller interval containing the minimum value, use the average value in the interval as the function variable, and use the Powell conjugate direction method to solve the global minimum value point. This method can be applied well to multivariate complex functions, avoiding the need to obtain partial derivatives [28].

After obtaining a set of optimal value points, it is also necessary to verify whether they are global minimum value points: directly substitute the initial values into the Powell method, compare the function values and variable values of the minimum points obtained twice, judge whether the obtained results are global optimal value solutions, and improve the overall solution quality and stability of the algorithm. In this way, the results obtained can comprehensively consider the original problem, where the objective function and the constraint conditions are both in the optimal state, and obtain the optimal values of the objective function and each variable.

After the optimization process, a set of values of  $d_1$ ,  $\theta_2$  and  $\theta_3$  are obtained, which can be substituted into Equation (10) to obtain the motion amount of each joint of the robotic arm, and realize the optimized motion control of the robotic arm.

#### 4. Structural Parameter Optimization of Robotic Arm

Within a certain range of the robotic arm length, longer robotic arm joints can meet more end pose angle requirements, and have a higher reachability; but at the same time, it will increase the possibility of damage to the tomato main stem and fruit during the whole branch machine's progress, resulting in a loss outweighing the gain. Therefore, it is necessary to optimize the design of some joints of the robotic arm, to ensure its reachability to all branch growth forms in the target whole branch space, while making the robotic arm structure as compact as possible.

The widely used industrial robotic arm groups in the current market meet all the branch work requirements, in terms of the reachability and compactness, with great difficulty. To complete the tomato branch pruning work efficiently, it is necessary to design a customized robotic arm configuration based on the working conditions, and the robotic arm geometric parameters are the key to the robotic arm configuration. Use the specified spatial position point and the whole branch end pose angle  $\alpha$  to measure the robotic arm's reachability to the spatial branch growth form, and use the two moving pair lengths  $d_1$  and  $d_4$  of the robotic arm to measure the compactness of the whole branch machine.

Optimize the design of  $d_1$  and  $d_4$ : Take the slide rail length  $d_1$  and the maximum extension amount  $d_4$  of the telescopic joint as the optimization objectives, and establish the corresponding mathematical model and constraint conditions. The extension length of joint 1 is determined by  $x_t$ ,  $y_t$  and  $z_t$  together, and the expression of the extension length  $d_1$  of joint 1 can be simplified as

$$f_1 = d_1(x_t, y_t, z_t) \quad (14)$$

According to the configuration of the robotic arm and the content in Section 2.2, the translation distance of joint 4 can be obtained as

$$d_4 = \sqrt{(x_t - x_4)^2 + (y_t - y_4)^2 + (z_t - z_4)^2}$$

where  $(x_t, y_t, z_t)$  are the coordinates of the whole branch target operation point,  $(x_4, y_4, z_4)$  are the coordinates of the origin of the coordinate system fixed on joint 4 in the robotic arm base coordinate system, and according to Equation (3),  $(x_4, y_4, z_4)$  are expressed by  $d_1, \theta_2$

and  $\theta_3$ . Therefore, the extension length of joint 4 is determined by  $x_t$ ,  $y_t$  and  $z_t$  together, and the expression of the extension length  $d_4$  of joint 4 can be simplified as

$$f_2 = d_4(x_t, y_t, z_t) \quad (15)$$

Combining Equations (14) and (15), the optimization objective is obtained as

$$\min F(x_t, y_t, z_t) = \{d_1(x_t, y_t, z_t), d_4(x_t, y_t, z_t)\}$$

To solve the optimal solution of the two objective functions in the value space, the parameters should be restricted according to the actual situation when establishing the mathematical model. The slide rail length  $d_1$  and the maximum extension amount  $d_4$  of the telescopic joint are subject to the following constraints:

1. The angle between the pruning claw and the branch, and the absolute value of the angle between the Z-axis of the robotic arm end and the branch direction should be greater than 30 degrees. The theoretical inverse solution method is combined to eliminate the impossible whole branch work situations, and to avoid extreme solutions in the optimization process. Where the angle between the two vectors is greater than  $30^\circ$ , this can be expressed as the range of the angle between the two vectors being  $30^\circ$ – $150^\circ$ .
2. The motion range of the rotary joint: The robotic arm is composed of multiple rotary joints; each joint has its own motion limit, and the influence of the robotic arm configuration is considered. This means that when the robotic arm performs pruning operations, it needs to consider the motion range of the joint, as shown in Equation (16), to avoid exceeding its allowable range during the motion process.

$$s.t. \begin{cases} \alpha \in (\frac{\pi}{2} \pm \sigma) \\ d_1, d_4 \geq 0 \\ -\pi/2 \leq \theta_2 \leq \pi/2 \\ 0 \leq \theta_3 < \pi/2 \end{cases} \quad (16)$$

where  $\sigma$  is the complement angle of  $30^\circ$ , which is  $60^\circ$ . Randomly generate 1000 spatial points in the target whole branch space to characterize all possible whole branch target points, and for each spatial point, there are 210 fixed spatial vectors to characterize the possible growth direction of the branch. Use the optimization mathematical model to solve these situations, and comprehensively obtain the optimal arm length in the global situation.

This model is regarded as a minimax problem, and the optimization is completed by using the relevant multi-objective optimization function, and a set of minimization points of the maximum value of the objective function is found. The minimax problem refers to finding a variable that makes the maximum value of multiple objective functions the smallest under some linear or nonlinear constraints, and can deal with complex multi-objective optimization problems under both linear and nonlinear constraints [29]. The result is  $d_{1max} = 953.149$  mm,  $d_{4max} = 632.320$  mm.

## 5. Experiment and Result

### 5.1. Verification of Optimal Structural Parameter

In Section 4, the maximum arm length parameters of the two robotic arms, the slide rail and the telescopic joint, were optimized, and the optimal values of the two arm length parameters were determined. To verify the uniqueness and validity of the optimal parameter solution, it is necessary to explore the change relationships between the optimization objective function and each variable, respectively.

The whole branch reachability  $v$  is used as the optimization evaluation index: the robotic arms with different arm length combinations are used to simulate the whole branch pruning for 210,000 kinds of branch growth forms, respectively. If the robotic arm end can reach the specified whole branch space point and the end pose angle can meet the whole

branch requirements, then this situation is counted as a successful whole branch situation, and the proportion of the successful whole branch results is calculated, which is expressed as the whole branch reachability  $v$ , to measure the whole branch reachability of the current arm length through the combination of the whole branch and robotic arm. The experiment verification process is as follows:

- (1) Fix one arm length and explore the effect of the other arm length on the reachability.
- (2) Solve the inverse kinematics of the robot for a certain branch position.
- (3) Use the robot forward kinematics to solve the end point and end vector based on the inverse solution.
- (4) Use mathematical methods to verify that the shear points coincide and the end branch angle meets the requirements.
- (5) Complete steps (2)–(4) for all branch growth forms, recording the proportion of reachable situations to measure the reachability of the current arm length combination.
- (6) Change the arm length, repeat steps (2)–(5) to obtain the relationship between the reachability and the arm length change.

Set  $d_1$  and  $d_4$  as the optimal results, respectively, and examine whether the other optimization objective changes the whole branch reachability within the value range of each configuration parameter, so as to transform this multi-objective optimization problem into a single-objective optimization for comparison verification.

### 5.2. Workspace Reachability of the Pruning Arm

In Sections 3 and 4, the pruning posture of the tomato pruning robotic arm and two key structural parameters were optimized, respectively, so that the pose matrix of each branch could correspond to solve for a unique end effector pose of the manipulator. To verify the overall reachability of the robotic arm in the target pruning workspace, simulation experiments are needed to test the effectiveness of the optimization method and whether the end effector pose of the arm can achieve the expected pruning effect, thereby providing a theoretical basis for the actual control of the manipulator.

In the simulation experiments, based on the actual spatial position of the branches in the manipulator coordinate system, the pose of the branches was simulated as the input parameter of the optimization function to solve for the optimal inverse kinematics of the robotic arm. The manipulator was then controlled to move based on the inverse solutions. It only needed to determine whether the end point of the arm could reach the cutting point of the side branch, and whether the angle between the end effector and the branch vector met the pruning requirements, to judge the reachability of the manipulator for the current side branch growth form. Finally, the reachability of the robotic arm for all the branch directions in the target pruning workspace was merged and summarized to measure the effective working area of the current arm.

### 5.3. Results and Discussion

To validate the effectiveness of the optimized robotic arm length,  $d_1$  and  $d_4$  were fixed at their optimal values, respectively, while the other variable was varied to examine its effect on the reachability.

When the maximum sliding joint's length  $d_1$  is fixed at 632.320 mm, the curve of the whole branch reachability  $v$  with the maximum extension length  $d_4$  of the telescopic joint is shown as follows.

As shown in Figure 6, the change in the maximum extension length of the telescopic joint has a significant effect on the reachability of pruning. When  $d_4$  is less than 630 mm, the reachability of pruning increases significantly as  $d_4$  increases. However, when  $d_4$  is greater than 630 mm, the reachability of pruning stabilizes at around 89.98%, indicating that the optimal  $d_4$  value appears in the range above 630 mm. When  $d_4 = 632.320$  mm, the reachability of pruning  $v$  first reached the maximum value of 89.98%. Therefore,  $d_4 = 632.320$  is reasonable. Further increasing the maximum extension length of the telescopic joint can hardly have a significant impact on the reachability and efficiency of pruning, but it increases

the volume of the robotic arm and the possibility of damaging the tomatoes' main stems and fruits during pruning. Therefore, the current optimized  $d_4$  result has been proven to be effective.

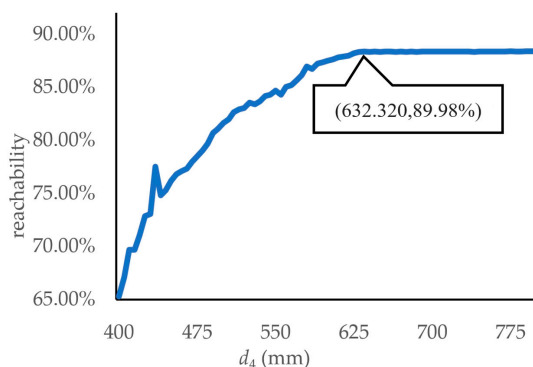


**Figure 6.** Reachability of pruning as maximum extension length of telescopic joint changes.

When the maximum extension length of the telescopic joint is fixed at  $d_4 = 953.149$  mm, the curve of the optimization objective function, the reachability of pruning  $v$ , varying with the maximum travel length of the sliding joint  $d_1$ , is shown in the figure below.

As shown in Figure 7, when  $d_1$  is less than 895 mm, the reachability of pruning fluctuates but shows a slightly increasing trend overall. When  $d_1$  is between 895 and 970 mm, the reachability of pruning stabilizes at around 88.15%. However, when  $d_1$  is greater than 970 mm, the reachability decreases instead, indicating that the optimal  $d_1$  value appears in the range of 895–970 mm. Therefore,  $d_1 = 953.149$  is reasonable. Further increasing the maximum travel length of the sliding joint can hardly improve the reachability of pruning, but it increases the volume of the robotic arm and the possibility of damaging the tomatoes' main stems and fruits during pruning. Thus, the current optimized  $d_1$  result has been proven to be effective.

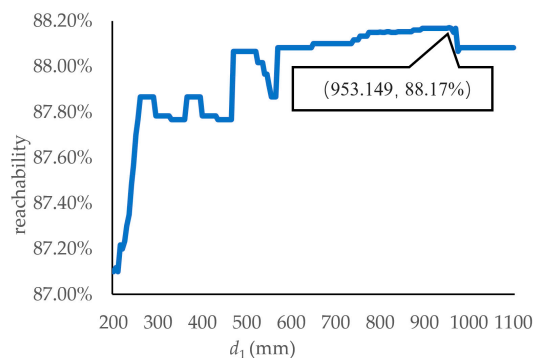


**Figure 7.** Reachability of pruning as maximum travel length of sliding joint changes.

In summary, the two optimization objectives are fixed as constants, respectively, to explore whether the other optimization objective has a unique optimal solution within the value range of each configuration parameter. By comparing the result ranges of each optimal configuration parameter, the final optimized parameter scheme is selected from the intersection, which can verify the effectiveness of this multi-objective optimization. That is, when  $d_1$  is 953.149 mm and  $d_4$  is 632.320 mm, the pruning robot can achieve the highest reachability in handling all the branch situations within the target pruning space, and the robotic arm system has the optimal motion performance and precision, better than other parameter combinations.

After obtaining the optimal combination of structural parameters, the working space needs to be further verified. Pruning simulations are performed on all possible branch direction vectors fixed to a point in the target pruning space, and the results of the current

pruning robot system's handling of branches in the space are shown in Figure 8. As the branch vectors in the space change, the angle of the end effector pose obtained by the pruning system will change accordingly. The reachability of pruning  $p$  is 89.94%.

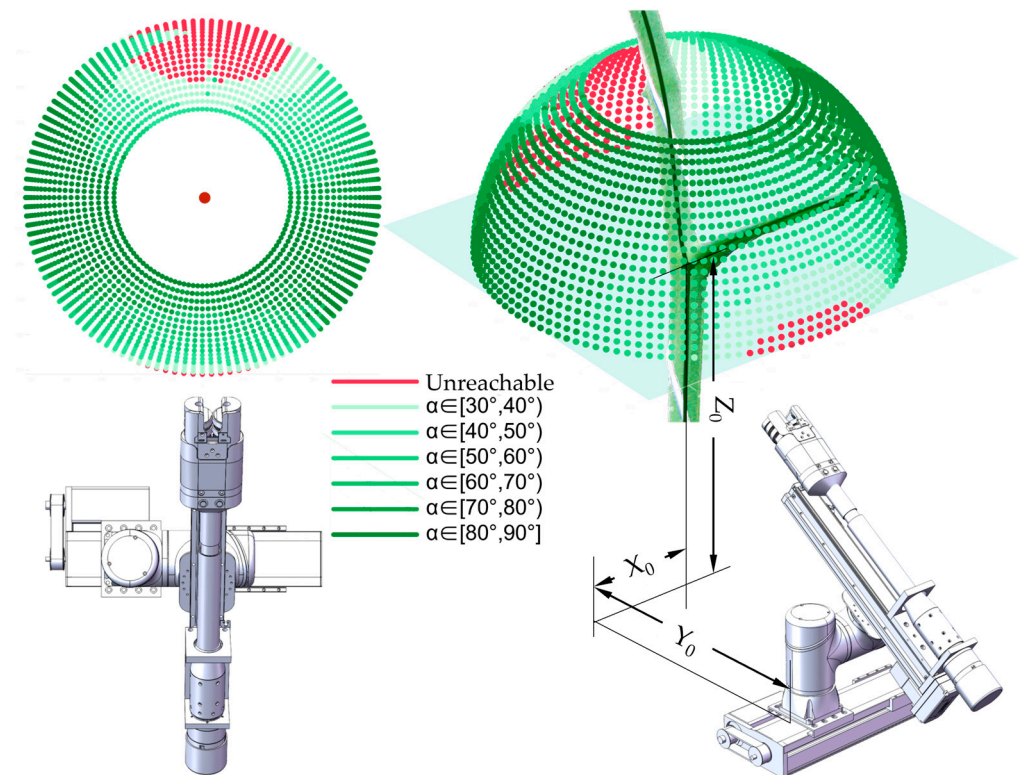


**Figure 8.** The whole branch reachable space of the optimized robotic arm.

The situations where the robotic arm is unreachable are mainly distributed in the vertical direction of the pruning robot: branches facing the pruning robot are concentrated in the space with a yaw angle of  $42^\circ$  and a pitch angle of  $6^\circ$ , accounting for 1.35%; branches in the same direction as the pruning robot are concentrated in the space with a yaw angle of  $57^\circ$  and a pitch angle of  $48^\circ$ , accounting for 8.71%. The branches that can achieve the optimal results are mostly distributed in the high pitch angle situations on the left, right and front sides of the pruning robot. The branches that can achieve the optimal results are mostly distributed in the high pitch angle situations on the left, right and front sides of the pruning robot.

Considering that the tomato pruning work requires the removal of 2–3 branches above the mature fruit each time, the current relatively compact robotic arm structure can achieve close to 90% reachability, which means that there may be one branch that cannot be pruned for every five tomato plants. However, this could be acceptable, because the impact of a small number of unpruned branches on light exposure, nutrient uptake and fruit yield is minimal.

In addition, the optimization method for the robotic arm structural parameters proposed in this paper is based on an important assumption that the main stem of the tomato is approximately upright. However, in the early research process of developing a visual identification model for branch pruning operation points [30], it was found that in actual greenhouse environments, the main stem may bend to some extent due to factors such as its own weight, plant support mode, and growth stage. This will lead to changes in the spatial position and orientation of the branches, thus affecting the reachability of the arm. This issue needs to be tested in the field after the robot is integrated to assess the pruning performance of the arm in real environments. At the same time, we also need to consider how to improve the structural design and control strategies of the arm to adapt to

the bending of the main stem, so as to further enhance the reachability and flexibility of the robotic arm.

## 6. Conclusions

A new dedicated PRRPR configuration pruning arm was designed for robotic tomato pruning, according to the pruning operation used in industrial greenhouses. The kinematic model of the robotic arm was determined. And the inverse kinematics solution method was proposed with the max angle between the branch and the end effector as the goal, to ensure that the branch could be pruned at its bottom with less stubble. With “pruning reachability” as the performance indicator, an optimization function was established to optimize the two key structural parameters of the pruning arm. The final optimization results are as follows: the maximum travel length  $d_1$  of the sliding joint is 953.149 mm, and the maximum extension length  $d_4$  of the telescopic joint is 632.320 mm. And the optimal solutions of the two optimization objectives have unique validity within the value range of the constituent parameters, achieving the design goals of maximizing the reachability of the pruning target positions and minimizing the structure size of the tomato pruning robot. The optimized manipulator could reach 89.98% of the side shoot growth positions in the pruning space with an end effector posture that meets the pruning requirements. This study could strongly support the future research and development of pruning robots.

**Author Contributions:** Conceptualization, Y.M. and Q.F.; methodology, Y.M. and Q.F.; software, Y.M. and W.Z.; validation, Y.M., Q.F. and X.G.; formal analysis, Y.M., Y.S. and B.W.; investigation, Y.M. and Y.S.; resources, Q.F.; data curation, Y.M. and Y.S.; writing—original draft preparation, Y.M.; writing—review and editing, Q.F.; visualization, Y.M.; supervision, Q.F.; project administration, L.C.; funding acquisition, Q.F. All authors have read and agreed to the published version of the manuscript.

**Funding:** This work was supported by the Beijing Nova Program (grant number 20220484023); the BAAFS Innovation Capacity Building Project (grant number KJCX20210414 and KJCX20240502).

**Institutional Review Board Statement:** Not applicable.

**Data Availability Statement:** The original contributions presented in the study are included in the article; further inquiries can be directed to the corresponding authors.

**Conflicts of Interest:** The authors declare that this study received funding from the Beijing Nova Program and the BAAFS Innovation Capacity Building Project. The funder was not involved in the study design, collection, analysis, interpretation of the data, the writing of this article or the decision to submit it for publication.

## References

- Li, J.; Xiang, C.; Wang, X.; Guo, Y.; Huang, Z.; Liu, L.; Li, X.; Du, Y. Current Situation of Tomato Industry in China During ‘The Thirteenth Five-year Plan’ Period and Future Prospect. *China Veg.* **2021**, *41*, 13–20. [CrossRef]
- Gatahi, D.M. Challenges and opportunities in tomato production chain and sustainable standards. *Int. J. Hortic. Sci. Technol.* **2020**, *7*, 235–262. [CrossRef]
- Sun, J.; Li, H.; Duan, Z. Morphological and Anatomical Observation of *Lycopersicon Esculentum* Branching. *Henan Sci.* **2014**, *32*, 726–729. [CrossRef]
- Turnbull, C.G. Shoot architecture II: Control of branching. *Annu. Plant Rev. Online* **2018**, *17*, 92–120. [CrossRef]
- Galliani, B.M. Plant Lateral Organs: Development, Growth and Ufe Span. DIPARTIMENTO DI BIOSCIENZE, 10 December 2018. 30 Ciclo, Anno Accademico 2017. 2018. Available online: <https://air.unimi.it/handle/2434/595119> (accessed on 19 November 2023).
- Maboko, M.; Du Plooy, C. Effect of pruning on yield and quality of hydroponically grown cherry tomato (*Lycopersicon esculentum*). *S. Afr. J. Plant Soil.* **2008**, *25*, 178–181. [CrossRef]
- Kumar, K.; Singh, D.; Saini, P.K.; Yadav, R. Progress in pruning to vegetable crops: A review. *Int. J. Adv. Agric. Sci. Technol.* **2019**, *6*, 19–32. [CrossRef]
- Wang, B.; Zhang, W.; Feng, Q. Measurement and Analysis of Mechanical Properties of Stem Clamping for Automatic Pruning of Tomato. *J. Agric. Mech. Res.* **2023**, *45*, 157–163. [CrossRef]
- Zhang, W.; Zhang, W.; Feng, Q.; Cheng, W.; Wang, B. Tomato Main-stem Tracking Control Method Based on PTZ Camera. *J. Southwest China Norm. Univ. (Nat. Sci. Ed.)* **2022**, *44*, 216–225. [CrossRef]

10. Panno, S.; Davino, S.; Caruso, A.G.; Bertacca, S.; Crnogorac, A.; Mandić, A.; Noris, E.; Matić, S. A review of the most common and economically important diseases that undermine the cultivation of tomato crop in the mediterranean basin. *Agronomy* **2021**, *11*, 2188. [[CrossRef](#)]
11. Botterill, T.; Paulin, S.; Green, R.D.; Williams, S.; Lin, J.; Saxton, V.; Mills, S.; Chen, X.; Corbett-Davies, S. A Robot System for Pruning Grape Vines. *J. Field Robot.* **2017**, *34*, 1100–1122. [[CrossRef](#)]
12. Huang, C.; Cai, D.; Wang, W.; Li, J.; Duan, J.; Yang, Z. Development of an automatic control system for a hydraulic pruning robot. *Comput. Electron. Agric.* **2023**, *214*, 108329. [[CrossRef](#)]
13. Verbiest, R.; Ruysen, K.; Vanwalleghem, T.; Demeester, E.; Kellens, K. Automation and robotics in the cultivation of pome fruit: Where do we stand today? *J. Field Robot.* **2020**, *38*, 513–531. [[CrossRef](#)]
14. Kroneman, W.; Valente, J.; Stappen, A.F.V.D. A fast two-stage approach for multi-goal path planning in a fruit tree. In Proceedings of the 2023 IEEE International Conference on Robotics and Automation (ICRA), London, UK, 29 May–June 2023; pp. 1586–1593.
15. Kaljaca, D.; Mayer, N.; Vroegindewei, B.A.; Mencarelli, A.; Henten, E.J.v.; Brox, T. Automated Boxwood Topiary Trimming with a Robotic Arm and Integrated Stereo Vision. In Proceedings of the 2019 IEEE/RSJ International Conference on Intelligent Robots and Systems (IROS), Macau, China, 3–8 November 2019; pp. 5542–5549. [[CrossRef](#)]
16. Li, Y.-R.; Lien, W.-Y.; Huang, Z.-H.; Chen, C.-T. Hybrid Visual Servo Control of a Robotic Manipulator for Cherry Tomato Harvesting. *Actuators* **2023**, *12*, 253. [[CrossRef](#)]
17. Cuevas-Velasquez, H.; Gallego, A.J.; Tylecek, R.; Hemming, J.; Tuijl, B.v.; Mencarelli, A.; Fisher, R.B. Real-time Stereo Visual Servoing for Rose Pruning with Robotic Arm. In Proceedings of the 2020 IEEE International Conference on Robotics and Automation (ICRA), Paris, France, 31 May–31 August 2020; pp. 7050–7056.
18. Arad, B.; Balendonck, J.; Barth, R.; Ben-Shahar, O.; Edan, Y.; Hellström, T.; Hemming, J.; Kurtser, P.; Ringdahl, O.; Tielen, T.; et al. Development of a sweet pepper harvesting robot. *J. Field Robot.* **2020**, *37*, 1027–1039. [[CrossRef](#)]
19. Kootstra, G.; Wang, X.; Blok, P.M.; Hemming, J.; van Henten, E. Selective Harvesting Robotics: Current Research, Trends, and Future Directions. *Curr. Robot. Rep.* **2021**, *2*, 95–104. [[CrossRef](#)]
20. Zhao, Q.; Li, L.; Wu, Z.; Guo, X.; Li, J. Optimal Design and Experiment of Manipulator for Camellia Pollen Picking. *Appl. Sci.* **2022**, *12*, 8011. [[CrossRef](#)]
21. Xiong, Z.; Feng, Q.; Li, T.; Xie, F.; Liu, C.; Liu, L.; Guo, X.; Zhao, C. Dual-Manipulator Optimal Design for Apple Robotic Harvesting. *Agronomy* **2022**, *12*, 3128. [[CrossRef](#)]
22. Feng, Q.; Ji, C.; Zhang, J.; Li, W. Optimization design and kinematic analysis of cucumber-harvesting-robot manipulator. *Nongye Jixie Xuebao/Trans. Chin. Soc. Agric. Mach.* **2010**, *41*, 244–248. [[CrossRef](#)]
23. Molaei, F.; Ghatrehsamani, S. Kinematic-Based Multi-Objective Design Optimization of a Grapevine Pruning Robotic Manipulator. *AgriEngineering* **2022**, *4*, 606–625. [[CrossRef](#)]
24. Roshanianfard, A.; Mengmeng, D.; Nematzadeh, S. A 4-DOF SCARA Robotic Arm for Various Farm Applications: Designing, Kinematic Modelling, and Parameterization. *Acta Technol. Agric.* **2021**, *24*, 61–66. [[CrossRef](#)]
25. Özgür, E.; Mezouar, Y. Kinematic modeling and control of a robot arm using unit dual quaternions. *Robot. Auton. Syst.* **2016**, *77*, 66–73. [[CrossRef](#)]
26. Lasdon, L.; Waren, A.; Rice, R. An interior penalty method for inequality constrained optimal control problems. *IEEE Trans. Autom. Control* **1967**, *12*, 388–395. [[CrossRef](#)]
27. Liu, R.; Wang, Q. A Golden Section Method for Univariate One-Dimensional Maximum Likelihood Parameter Estimation. In Proceedings of the Communications, Signal Processing, and Systems, Singapore, 20–22 July 2019; pp. 2571–2580.
28. Ibrahim, A.M.; Tawhid, M.A. Conjugate direction de algorithm for solving systems of nonlinear equations. *Appl. Math. Inf. Sci.* **2017**, *11*, 339–352. [[CrossRef](#)]
29. Taha, K. Methods that optimize multi-objective problems: A survey and experimental evaluation. *IEEE Access* **2020**, *8*, 80855–80878. [[CrossRef](#)]
30. Feng, Q.; Cheng, W.; Li, Y.; Wang, B.; Chen, L. Method for identifying tomato plants pruning point using Mask R-CNN. *Trans. Chin. Soc. Agric. Eng.* **2022**, *38*, 128–135. [[CrossRef](#)]

**Disclaimer/Publisher’s Note:** The statements, opinions and data contained in all publications are solely those of the individual author(s) and contributor(s) and not of MDPI and/or the editor(s). MDPI and/or the editor(s) disclaim responsibility for any injury to people or property resulting from any ideas, methods, instructions or products referred to in the content.